Proceedings of the 2003 IEEE International Frequency Control Symposium and PDA Exhibition Jointly with the 17th European Frequency and Time Forum

MICROOPTOELECTROMECHANICAL SYSTEMS AND FREQUENCY CONTROL

Sergey Edward Lyshevski [1] and Marina Alexandra Lyshevski[2]
[1]Department of Electrical Engineering, Rochester Institute of Technology, Rochester, NY 14623-5603, USA
[2]Department of Chemistry, Rochester Institute of Technology, Rochester, NY 14623, USA
E-mail: seleee@rit.edu, Web: www.rit.edu/~seleee

Abstract – **Wireless communication remains on the forefront of current systems because reliable and robust communication is needed to guarantee the system functionality, operationability, integrity, etc. Significant progress has been made. However, formidable challenges remain and novel design concepts are sought. Fundamental research in optical wireless communication and discovery of novel nonmechanical beam steering concepts ensure promising revolutionary changes. The technologies are available to fabricate the microoptoelectro-mechanical systems (MOEMS). For example, in addition to CMOS and fiber optics, surface micromachining has been used to fabricate micro- and miniscale lasers, mirrors, photodiodes, lenses, etc. The MOEMS-based optical wireless communication systems have been applied for fiber switching, scanning, beam steering, projection, pointing, etc. Different microstructures and microdevices (mirrors, lenses, magnets, antennas, actuators, etc.) are the components of MOEMS. We devise and examine novel MOEMS that integrate vertical cavity surface emitting laser (VCSEL), active optoelectromagnetic microdevices (Bragg cells and optoelectromagnetic lenses), radiating energy microdevices (antennas) and controlling/processing integrated circuits (ICs). The MOEMS designed utilize the Microsystem-on-Chip paradigm. High-fidelity modeling, heterogeneous simulation, data-intensive analysis and optimization are performed. These fundamental problems directly related and contribute to newly emerging fields of computational optoelectromagnetics and optoelectromechanics. Data-intensive analysis and high-fidelity modeling are important part in synthesis and design of affordable high-performance MOEMS. This paper focuses on the development of the theory of computational optoelectromagnetics and CAD of MOEMS. The modeling, simulation, analysis and design results are reported and illustrated. The major emphasis is given on nonmechanical beam steering paradigm utilizing devised MOEMS.**

Keywords **– analysis, control, modeling, MOEMS, VCSEL**

I. INTRODUCTION

The current trends towards systems synergy, integrity, functionality, adaptability, robustness, and versatility have facilitated the need for the development of systems with wireless communication capabilities [1, 2]. Some possible applications include wireless networks for complex cooperative multi-agent systems (manufacturing, fabrication processes, air traffic, etc.), stand-alone and interacting systems (aircraft, spacecrafts, cars, robots, ground and underwater vehicles, etc.), as well as microscale systems and devices. Different wireless communication systems have been designed and tested using active transmitters (emitting diodes and lasers) and passive transmitters (reflectors).

Mirror arrays, micromirrors, optical lenses, piezoelectric shutters, Kerr cells, Pockels cells, Bragg cells, liquid crystals and other devices have been used to reflect the emitted light. The recent analysis and trends clearly suggest that further advancements are needed. The application of MOEMS has been shown to be very promising. For MOEMS, electromechanical (mechanical) and optoelectromagnetic (nonmechanical) beam steering paradigms have been implemented and tested in [3-7] and [8-12], respectively. Fast steering, superior accuracy, high bandwidth, robustness, affordability and high efficiency can be accomplished utilizing the optoelectromagnetic paradigm. In this paper we examine the Bragg cells and optoelectromagnetic-based adaptive microlenses to attain nonmechanical beam steering in high-performance MOEMS.

The studied MOEMS integrate optical microdevices, microstructures, MEMS-based VCELS, radiating energy microdevices, and ICs. The major challenges in MOEMS are to guarantee the desired performance level and enhanced functionality while minimizing size, reducing complexity, maximizing efficiency, integrity and robustness. This paper reports devised MOEMS with MEMS-based VCSEL that can be fabricated using CMOS and surface micromachining technologies. These affordable MOEMS can be used in wireless communication, laser scanners, optical interconnects, etc. The beam steering is achieved utilizing electro-acoustic and optoelectromagnetic steering controlling the electromagnetic field that changes the refractive index and acoustic frequency. High-fidelity modeling and data-intensive analysis are reported.

II. MICROOPTOELECTROMECHANICAL SYSTEMS WITH ACTIVE OPTICS

High-performance MOEMS are designed, and MEMS-based multiple wavelength VCSEL are integrated with active optics. Nonmechanical beam steering can be performed by changing the wavelength and refractive index of the optical media. The wavelength of the MEMS-based VCSEL can be controlled by varying the length of cavity, while the refractive index is a function of the electromagnetic field. The radiating energy microdevice (antenna) varies the electromagnetic field, and the voltages are changed using high-frequency ICs. Figure 1 illustrates

the System-on-Chip MOEMS that utilize MEMS-based electromechanical [3-7] and optoelectromagnetic paradigms that lead to mechanical and nonmechanical beam steering, respectively.

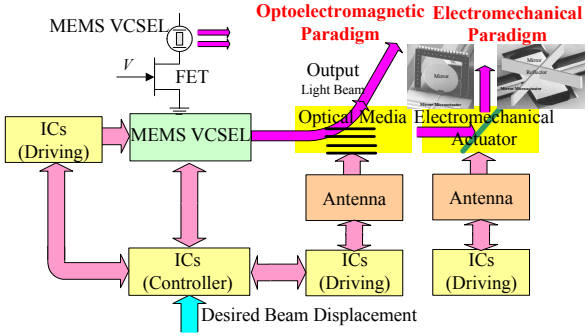

Figure 1. MOEMS configurations

2.1. Electromechanical-Based MOEMS

Electromagnetic and electrostatic microactuators and scanning micromirrors for electromechanical-based mechanically steered MOEMS can are made using surface micromachining [3-7, 13]. Fast and precise positioning is achieved using high-performance rotating microactuators controlled by ICs that implement pulse-width-modulation concept with high switching frequency [13]. The experimental studies show that the settling time for the angular positioning is microseconds without overshoot. In addition to actuation (angular positioning) of micromachined micromirrors, the motion and deformation of scanning micromirrors as well as accurate sensor technology must be addressed and studied [13]. For perfectly flat mirrors, the far-field beam divergence is due to the diffraction effect (finite mirror size). However, stress-induced mirror curvature causes beam divergence that degrades the performance [13]. Novel deposition processes and materials have been used to minimize this effect (surface micromachined mirrors are fabricated using CMOS deposition processes and material usually have unacceptable static curvature after release). The overall performance of the Microsystem-on-Chip depends upon the performance of all components, e.g., actuators, sensors, mirror, ICs and VCSEL. Advanced deposition and polishing processes are applied to guarantee a few tens of nanometers commonplace and roughness of micromirrors [3-7]. However, micromirror deformations, due to thin-film stresses, elasticity, flexibility, drag, resonance and other electro-mechanical phenomena, cause serious performance degradation. The ability to characterize, analyze, control and minimize dynamic deformation effects is therefore crucial to the development of high-performance MOEMS. The dynamic micromirror deformations, occurred when the mirror is actuated, can be minimized increasing the micromirror thickness. However, this leads to increase of the moment of inertia, application of high-torque microactuators and high current ICs. This leads to increased settling time, high power, etc. Hence, other paradigms should be considered. We propose the opto-electromagnetic nonmechanical steering concepts that result in the design of high-performance System-on-Chip MOEMS.

2.2. Optoelectromagnetic-Based MOEMS

Due to the well-known deficiencies of the mechanical-based beam steering MOEMS, as were briefly summarized in section 2.1, this paper concentrates on the optoelectromagnetic nonmechanical steering concepts that based on the application of active optical media, e.g., Bragg cells and optoelectromagnetic microlenses. Utilizing the acousto-optic effect, the Brag cells change the beam angle. The deflection angle, as a function of the acoustic frequency, is given as

$$\theta_D = \frac{\lambda f}{nv} - 2\theta_B ,$$

where λ is the wavelength of the VCSEL beam; f is the acoustic frequency of the traveling acoustic wave in the Bragg cell; n is the index of refraction; v is the acoustic velocity; θ_B is the Bragg angle for the incident beam, $\theta_B = \frac{\lambda f_c}{2nv}$; f_c is the center frequency of the Bragg cell.

The MOEMS that utilize Bragg cells are perfectly suited to deflect the beam in one dimension within the limited deflection angle, and the acoustic frequency is in the range of 40 MHz. The alternative MOEMS can be designed using active optoelectromagnetic microlenses that vary the geometry by applying the electromagnetic field or utilize the organic and inorganic materials that change the refractive index under the applied electromagnetic field [8-11].

MOEMS control (with ultimate objective to accurately steer the beam, e.g., to perform position tracking) should be solved performing modeling, simulations and analysis. To solve these sequential problems, mathematical modeling is addressed, and high-fidelity models are derived. These partial differential equations are used to perform heterogeneous simulations and data-intensive analysis using MATLAB. High-accuracy super-fast beam steering (positioning) is achieved designing intelligent controllers. The controller (implemented using ICs) regulates the voltage applied to the antenna to control the electromagnetic field in the optically active media to deflect the beam. Different MOEMS components are studied in the following section for the proposed System-on-Chip MOEMS configuration that was documented in Figure 1.

III. VERTICAL-CAVITY SURFACE-EMITTING LASERS

Vertical-cavity surface-emitting lasers have been researched extensively as key components for next-generation of wireless communication, computing, processing, switching, and optical devices. The aluminum gallium arsenide (AlGaAs) and gallium arsenide (GaAs) VCSELs have the emission wavelengths below 1 μm (typically 650, 780, 820 and 850 nm), and these lasers have demonstrated good performance [14-16]. In addition to these medium-wavelength lasers, the long-wavelength (emission

wavelengths 1.3 μm and higher), tunable and multiple-wavelength VCSELs are very important and needed to be designed. The indium gallium arsenide nitride (InGaAsN) VCSELs guarantee high-speed data and bandwidth, long distance capabilities, and silicon compatibility (silicon is transparent to 1.3 μm wavelength).

Conventional VCSELs integrate two oppositely doped distributed Bragg reflectors (DBR) with a cavity layer between them. At the center of the cavity layer there is an active region (multiple quantum wells). Current is injected into the active region using oxide or proton-implanted apertures. Recent research and developments have been progressed to the tunable, long-wavelength, and multiple-wavelength MEMS-based electrically- or optically-pumped VCSELs which integrate a bottom n-GaAs-AlGaAs DBR, a cavity layer with InGaAs active region, and a top mirror (p-DBR with AlAs and AlGaAs oxidation and sacrificial layers – air gap – top n-DBR suspended above the laser cavity and controlled by the microactuator). Hence, laser and MEMS are integrated. Recently, novel MEMS VCSELs topologies and configurations have been devices. These meaningful concepts will lead to essential improvement of lasers optimizing their performance.

VCSELs, fabricated using the CMOS technology, have the following advantages: high efficiency, emit light as a circular output beam vertically from the wafer surface with low divergence, integratability in two-dimensional array configurations, low threshold currents enabling high-density arrays, surface-normal emission (easy alignment and packaging), no need for corrective optics due to circular low divergence beams, lower temperature sensitivity (compared with edge-emitting lasers), very high bandwidth, low power consumption, affordability, high-yield fabrication, etc. Semiconductor lasers are based on the electron transmission involving annihilation of electrons and holes in semiconductors. In VCSEL the cavities are vertical to the semiconductor substrate (GaAs), see schematic diagram of the VCSEL in Figure 2. The lateral *p-n* junction is formed via epitaxial grow of the silicon-doped gallium-arsenide layers on the gallium-arsenide substrate. The formed *p-n* junction leads to the direct injection of electrons and holes into the double quantum well InGaAs active layer, and then directing the electrons through the higher bandgap DBR. The VCSELs can be integrated with the ICs as illustrated in Figure 1. Due to complicated epitaxial structures and material requirements, VCSELs are usually fabricated using metal-organic chemical vapor deposition (MOCVD). For the VCSEL illustrated in Figure 2, the vertical stripe in the center of the photo is the laser waveguide. 1550 nm wavelength infrared light is emitted from the ends of the waveguide. The large (dominating) region is the contact metalization area, and the current is supplied using two 1 mm horizontal gold wires. The VCSELs are the preferable choice for high-speed data communication allowing one to achieve more than 5 GHz frequency.

The analysis of the transient dynamics, documented in Figure 2 for 1 GHz step modulation, illustrates that the critically damped behavior on the rising edge of the beam output intensity and excellent jitter characteristics are achieved. In particular, the dynamics of the 1550 nm unpolarized VCSEL illustrates that 300 picoseconds rise and 1 nanoseconds fall settling times are achieved. The multiple spatial (transverse) modes of VCSELs are observed in the near-field image (logarithmic intensity map of the laser light at the emitting surface), see a near-field image of the Honeywell VCSEL demonstrated in Figure 2 [14, 16].

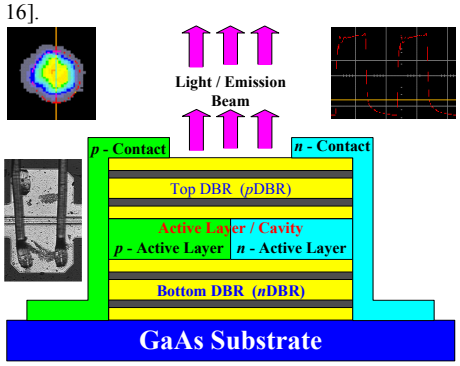

Figure 2. Schematic diagram of a VCSEL

The proposed solution offers gigabit per second transmission data rate guaranteeing superior bandwidth. Innovative MEMS VCSELs with the suspended top mirror (deformable membrane suspended above the semiconductor) and variable airgap are discussed, modeled and analyzed. The laser light beam should be accurately pointed, and the active optics such as Bragg cells and tunable optoelectromagnetic mirrors are considered.

IV. Optoelectromagnetic Micromirror

Different paradigms have been developed to utilize optoelectrical and optoelectromagnetic phenomena to reflect the light. References [8-12] provide different meaningful solutions that have advantages and drawbacks. We consider the microlens as illustrated in Figure 3. It is evident that the proposed microlens utilizes the optoelectromagnetic phenomena. The electromagnetic field can be varied by changing the voltages applied to the electrodes. It should be emphasized that in addition to changing the microlens geometry, the refractive index can be changed.

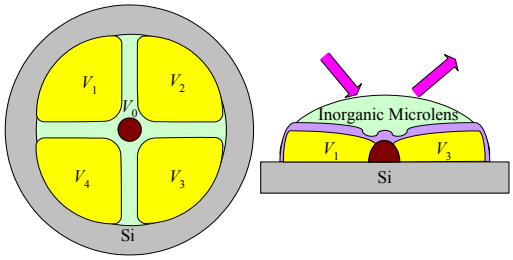

Figure 3. Optoelectromagnetic microlens with antenna

V. Mathematical Model For MOEMS

To model the integrated optoelectromagnetic phenomena and effects in the studied MOEMS, synergetic models must be developed and analyzed. Modeling, simulation, and analysis will lead to designing of MOEMS with the desired properties and attaining the superior performance (accurate beam pointing, maximal efficiency, enhanced robustness, minimal losses, power consumption, etc.). MOEMS have been modeled using different mathematical models. Due to complex optoelectromagnetic phenomena, the steady-state, linear concepts and finite element analysis do not allow one to comprehensively study MOEMS performance. It was illustrated that the studied MOEMS integrates many components, e.g., MEMS VCSEL, Bragg cell or active optoelectromagnetic microlenses, ICs, etc. All these sybsystems must be coherently studied and examined.

5.1. Computational Optoelectromechanics: High-Fidelity Modeling of MEMS-Based VCSELs

For VCSELs, equivalent circuit, Laguerre-Gaussian, single- and two-mode modeling, as well as other concepts have been applied. The deficiencies that cannot be overcome were reported in [14-16]. This paper overcomes the well-known limitations in modeling, simulation and analysis of MEMS VCSELs applying the basic equations with minimum level of simplifications and assumptions. These partial differential equations are solved in the time domain applying heterogeneous simulations, and numerical results are reported. It is illustrated that it is possible to integrate complex phenomena and effects in MEMS-based VCSELs and make analysis computationally tractable using the density functional theory and effective Maxwell's-Bloch equations. The tunable long-wavelength MEMS VCSELs are modeled, simulated and analyzed.

MEMS VCSELs integrate nanostructures and microactuators that must be modeled. The Schrödinger equation cannot be solved even for simple nanostrustures. Therefore, other paradigms are sought. The density functional theory can be applied to the one-dimensional (quantum well), two- and three-dimensional nanostructures that are the components of the studied MEMS-based VCSELs. The total energy of *N*-electron system under the external field is found using the three-dimensional charge density $\rho(\mathbf{r})$ as [13]

$$E\left(t,\rho(\mathbf{r})\right)=\underbrace{\Gamma_1\left(t,\rho(\mathbf{r})\right)+\Gamma_2\left(t,\rho(\mathbf{r})\right)}_{\text{kinetic energy}}+\underbrace{\int_{\mathbf{R}}\frac{e\rho(\mathbf{r}')}{4\pi\varepsilon|\mathbf{r}-\mathbf{r}'|}d\mathbf{r}'}_{\text{potential energy}},$$

where $\Gamma_1\left(t,\rho(\mathbf{r})\right)$ and $\Gamma_2\left(t,\rho(\mathbf{r})\right)$ are the interacting (exchange) and non-interacting kinetic energies of a single electron in *N*-electron *Z*-nucleus system,

$$\Gamma_1(t,\rho(\mathbf{r}))=\int_{\mathbf{R}}\gamma(t,\rho(\mathbf{r}))\rho(\mathbf{r})d\mathbf{r}$$

and $\Gamma_2(t,\rho(\mathbf{r}))=-\frac{\hbar^2}{2m}\sum_{j=1}^{N}\int_{\mathbf{R}}\psi_j^*(t,\mathbf{r})\nabla^2\psi_j(t,\mathbf{r})d\mathbf{r}$;

$\gamma\left(t,\rho(\mathbf{r})\right)$ is the parameterization function.

The problem of modeling of *N*-electron *Z*-nucleus systems becomes equivalent to the solution of the equation for one electron. The Kohn-Sham electronic orbitals are subject to the following orthogonal condition

$$\int_{\mathbf{R}}\psi_i^*(t,\mathbf{r})\psi_j(t,\mathbf{r})d\mathbf{r}=\delta_{ij}.$$

The charge density is found taking note of the Schrödinger equation, and the first-order Fock-Dirac electron charge density matrix is

$$\rho_e(\mathbf{r})=\sum_{j=1}^{N}\psi_j^*(t,\mathbf{r})\psi_j(t,\mathbf{r}).$$

The three-dimensional electron charge density is a function of three variables (*x*, *y* and *z* in the Cartesian coordinate system). Integrating the electron charge density $\rho_e(\mathbf{r})$, one obtains the charge of the total number of electrons *N*, e.g., $\int_{\mathbf{R}}\rho_e(\mathbf{r})d\mathbf{r}=Ne$.

Hence, $\rho_e(\mathbf{r})$ satisfies the following properties

$\rho_e(\mathbf{r})>0$,

$\int_{\mathbf{R}}\rho_e(\mathbf{r})d\mathbf{r}=Ne$,

$\int_{\mathbf{R}}\left|\sqrt{\nabla\rho_e(\mathbf{r})}\right|^2 d\mathbf{r}<\infty$,

$\int_{\mathbf{R}}\nabla^2\rho_e(\mathbf{r})d\mathbf{r}=\infty$.

For the nuclei charge density, we have

$\rho_n(\mathbf{r})>0$

and $\int_{\mathbf{R}}\rho_n(\mathbf{r})d\mathbf{r}=\sum_{k=1}^{Z}q_k$.

There exist an infinite number of antisymmetric wavefunctions that give the same $\rho(\mathbf{r})$. The minimum-energy concept (energy-functional minimum principle) is applied. The total energy is a function of $\rho(\mathbf{r})$, and the so-called ground state Ψ must minimize the expectation value $\langle E(\rho)\rangle$.

The searching density functional $F(\rho)$, which searches all Ψ in the *N*-electron Hilbert space *H* to find $\rho(\mathbf{r})$ and guarantee the minimum to the energy expectation value, is

$$F(\rho)\le\min_{\substack{\Psi\to\rho\\ \Psi\in H_\Psi}}\left\langle\Psi\middle|E(\rho)\middle|\Psi\right\rangle,$$

where H_Ψ is any subset of the *N*-electron Hilbert space.

Using the variational principle, we have

$$\frac{\Delta E(\rho)}{\Delta f(\rho)}=\int_{\mathbf{R}}\frac{\Delta E(\rho)}{\Delta\rho(\mathbf{r}')}\frac{\Delta\rho(\mathbf{r}')}{\Delta f(\mathbf{r})}d\mathbf{r}'=0,$$

where $f(\rho)$ is the nonnegative function.

Thus, one concludes that $\left.\frac{\Delta E(\rho)}{\Delta f(\rho)}\right|_N=\text{const}$.

As the wavefunctions converge (the conditions of the Hellmann-Feynman theorem are satisfied), we have

$$\int_{\mathbf{R}} \frac{\partial E(t,\mathbf{r})}{\partial \rho(t,\mathbf{r})} \frac{\partial \rho(t,\mathbf{r})}{\partial \mathbf{r}_r} d\mathbf{r} = 0 .$$

The reported approach allows one to model optoelectromagnetic transient dynamics of micro- and nanostructures in VCSELs. The nonlinear Maxwell-Boltzmann-Poisson-Bloch and Navier-Stokes equations, which integrate complex phenomena, are used to model the VCSELs in the time domain. We use the following nonlinear Maxwell's-Bloch partial differential equations [15]

$$\frac{\partial E}{\partial t} = \frac{c}{n_g} j \left[\frac{\lambda}{4\pi n_p} \nabla^2 E - kE + \frac{\pi n_p \Gamma}{\lambda \varepsilon_0 \varepsilon_b} \left(\varepsilon_0 \varepsilon_b \chi_0(N) E + P \right) + \frac{2\pi C(x,y)}{\lambda} E \right],$$

$$\frac{\partial N}{\partial t} = \nabla D_N \nabla N - \gamma_n N + \frac{\eta J(x,y)}{e} + j \frac{L\Gamma}{8\hbar} \left[\left(\varepsilon_0 \varepsilon_b \chi_0(N_c) E + P \right)^* E - \left(\varepsilon_0 \varepsilon_b \chi_0(N) E + P \right) E^* \right],$$

$$\frac{\partial P}{\partial t} = \left[j(\omega_d - \omega(N_c)) - \Gamma(N_c) \right] P - j \varepsilon_0 \varepsilon_b A(N_c) E , \quad (1)$$

where E is the laser field; N_c is the two-dimensional carrier density; P is the induced polarization of the semiconductor media; ∇ represents the Laplacian operator in the transverse plane x and y; n_g and n_p are the ground and phase indices of refraction for no exited semiconductor; c is the speed of light; j is the complex number, $j=\sqrt{-1}$; λ is the wavelength; k is the cavity losses coefficient due to cavity transmission and background absorption; $C(x,y)$ is the two-dimensional confinement oxidation profile; D_N is the carrier diffusion constant; $J(x,y)$ is the injected current in the xy plane; ω_d is the detuning between reference and bandwidth frequencies; Γ, A, γ_0 and ω are the carrier-density dependent gain bandwidth, strength, effective susceptibility, and frequency (detuning) coefficients, respectively.

The set of nonlinear partial differential equations (1) augmented with the density functional concept results in high-fidelity mathematical models of MOEMS with MEMS VCSELs.

5.2. High-Fidelity Modeling of Electromagentic Field

The electromagnetic field is modeled using Maxwell's equations [13]. Different paradigms have been successfully applied to perform modeling relaxing the computational difficulties to make the problem computationally tractable. Using the boundary conditions, the solution is found using the Fourier transform method. We use the advanced MATLAB software and its toolboxes, e.g., the Partial Differential Equations toolbox. It is demonstrated that the complex electromagnetic phenomena and effects can be thoroughly examined by making use of numerical solutions based upon high-fidelity mathematical modeling paradigms.

VI. CONTROL OF MOEMS

High-performance MOEMS must be designed to achieve specified criteria, and developing novel control paradigms are vital. It is difficult (if not impossible) to apply high-fidelity mathematical models of MOEMS to solve the control problem in the classical formulation. Some majors problem the designer faces are:

1. large number of microscale devices and structures that exhibit very complex multivariable optoelectro-magnetic, opto-electrical and opto-electro-mechanical phenomena;
2. even high-fidelity mathematical models are idealization of complex phenomena and effects with the specified degree of simplifications and assumptions (linear and steady-state failed in the attempts to model MOEMS);
3. large-scale integration and complexity (for example ICs for VLSI may integrate thousands of FETs);
4. uncertainties and parameter variations;
5. disturbances, perturbations, etc.

Therefore, though high-fidelity mathematical models in the form of high-order partial differential equations can be developed to perform analysis and simulations (thousands equations result for MOEMS), control methods exhibit well-known difficulties and drawbacks [13, 17, 18]. Our goal is to design robust reconfigurable controllers that consistently and reliably exhibit evolutionary learning and adaptation. The reported *information-theoretic* design concept is based on logical implications of experimental evidence of MOEMS performance. In particular, a method in which the MOEMS performance is optimized with respect to available experimental evidence is documented.

The mathematical foundation of the reported *information-theoretic* design method is based on the optimization of MOEMS performance, and linear and nonlinear maps of the performance variables (measured, estimated or observed controls, references, states, outputs, and decision-making variables) are used in the synthesis. The performance functionals are minimized. We apply the criteria to search candidate controllers (design – implement – assess – optimize), and derive a *premium* controller, which guarantees optimal performance level with respect to all available past experimental evidence. To illustrate the procedure, we design the *premium* controller that learns and optimizes the MOEMS performance through adaptation, reconfigurations and tuning. Input and output variables are defined from the set of the performance variables (measured information set) that allow one to synthesize the objective functional to evaluate the performance status using the measured data.

6.1. Synthesis of Premium Controllers

Our goal is to design *premium* controllers utilizing evolutionary learning and adaptation mechanisms [17]. We intent to ensure learning and optimization through self-adaptation to optimize performance of closed-loop MOEMS using specified criteria (stability, accuracy, efficiency, reliability, robustness, etc.) and tasks (real-time decision making, assessment analysis, outcome prediction, diagnostics, etc.). For MOEMS, the performance,

functionality, goals, tasks and requirements can be studied as the relationships between controls (u), references (r), and outputs (y). In addition, the measured states and decision-making variables can be also integrated as y.

Based upon the quantitative and qualitative requirements, criteria and specifications, by using the triple of the measured performance variables $(r, y, u) \in R \times Y \times U$, the designer synthesizes objective functionals to examine the MOEMS performance. The MEMS performance and functionality are *mapped* using the performance variables, and the performance map is given by $p = f(u, r, y)$.

Controllers

$$u = K(r, y) \quad (2)$$

will be evaluated using performance objective functionals

$J_F: R \times Y \times U \to$ ú.

Using the objective functional and performance level $\gamma \in$ ú, we define the performance goal as

$J_F(r, y, u) \le \gamma, \forall r \in R$.

The desired performance is achieved if for all inputs the corresponding closed-loop response triples (r,y,u) lie in the set [17]

$$J_S(\gamma) \stackrel{\Delta}{=} \{(r, y, u) \in R \times Y \times U \mid J_F(r, y, u) \le \gamma\}.$$

Definition. For MOEMS, controller (2) is defined to be *improper* with respect to the performance level γ, if the measured data $\{(u_{data}(t), y_{data}(t) \mid t \in T\}$ is sufficient to deduce that the controller (2) cannot satisfy the performance goal $J_F(r, y, u) \le \gamma, \forall r \in R$ imposed on MOEMS. Otherwise controller (2) is defined to be *proper*. The *proper* control law (2) is the premium controller K_p for MOEMS if there is no other controller that is *proper* with respect to lesser performance level. ~

Our ultimate goal is to synthesize *premium* controllers for MOEMS. Using the *performance specification* $J_S(\gamma)$, *measurement data* M_S, and *controller* K_S sets, one can distinguish controllers according to their performance level γ[17, 18].

Theorem 1. For MOEMS, controller (2) is the *proper* control law with respect to performance level γ if and only if for each triple $(r_0, y_0, u_0) \in M_S \cap K_S$ there exists at least one pair (y_1, u_1) satisfying

$(r_0, y_1, u_1) \in M_S \cap K_S \cap J_S(\gamma)$,

where $J_S(\gamma) \stackrel{\Delta}{=} \{(r, y, u) \in R \times Y \times U \mid J_F(r, y, u) \le \gamma\}$,

$M_S \stackrel{\Delta}{=} \{(r, y, u) \in R \times Y \times U \mid u(t) = u_{data}(t), y(t) = y_{data}(t), \forall t \in T\}$,

$K_S \stackrel{\Delta}{=} \{(r, y, u) \in R \times Y \times U \mid u = K(r, y)\}$. ~

In MOEMS, the dependence of the performance objective functional $J_F(r, y, u)$ on the values of (y, u) is determined by $\{(u_{data}(t), y_{data}(t) \mid t \in T\}$. Theorem 2 allows one to synthesize *premium* controllers for MOEMS.

Theorem 2. For MOEMS, controller (2) is *proper* with respect to the performance level γ if and only if

$$M_S \cap K_S \cap \overline{J_S(\gamma)} = \emptyset.$$

The premium controller and its performance level γ_{opt} are found by solving the following optimization problem

$$\gamma_{\text{opt}} = \min_{K \in \mathbf{K}} \gamma \quad \text{subject to } M_S \cap K_S \cap \overline{J_S(\gamma)} \neq \emptyset$$

where $\mathbf{K}$ is the set of candidate controllers for MOEMS. ~

Here, $\overline{J_S(\gamma)}$ is the complement of the set $J_S(\gamma)$.

The elements of set $\overline{J_S(\gamma)}$ are triples (r, y, u) that violate the performance specification

$$J_S(\gamma) \stackrel{\Delta}{=} \{(r, y, u) \in R \times Y \times U \mid J_F(r, y, u) \le \gamma\}.$$

Thus,

$$\overline{J_S(\gamma)} \stackrel{\Delta}{=} \{(r, y, u) \in R \times Y \times U \mid J_F(r, y, u) > \gamma\}.$$

It is evident that the performance level γ_{opt} depends on:

1. measured input and output data $(u_{data}(t), y_{data}(t))$;
2. candidate controller set;
3. performance objective functional $J_F(r, y, u)$.

As the objective functional is given, the performance level γ_{opt} is a function of $(u_{data}(t), y_{data}(t))$ and candidate controller set. The controller (2) is *proper* if and only if there are no closed-loop response triples (r, y, u), consistent with both the controller relation K_S and the measured data, that violate the performance specification for MOEMS.

The objective functionals are synthesized as

$$J_F(r, u, y) = f_1(p) + \int_{t_0}^{t_f} f_2(p) dt,$$

where $p = f(u, r, y)$ is the performance map; f_1 and f_2 are the nonlinear maps of the MOEMS performance variables.

The control laws for MOEMS can be designed by

- examining different controllers K in the candidate controller set $\mathbf{K}$,
- eliminating K which do not satisfy the objective functional,
- reconfiguring controllers, and tuning the feedback gains.

A prearranged set of robust control laws with feedback gains which ensure stability in the worst-case scenarios can be used to initialize learning and search through adaptation process performed in real-time.

6.1. Synthesis of a Premium Controller for MOEMS

We study real-time evolutionary learning and adaptation (reconfiguration and tuning) for an optoelectromagnetic MOEMS. Using evolutionary learning and adaptation, the intelligent control problem should be solved without linguistic or mathematical models. The performance functional is $J_F(r, u, y) = f_1(p) + \int_{t_0}^{t_f} f_2(p) dt$, where performance integrands f_1 and f_2 should be designed. The objective functional, which measures the MOEMS performance, is

$$J_F(r,u,y)=$$

$$\min_i q_{11}\int_{t_0}^{t_f}|i|dt+\min_{t,e_\lambda} q_{12}\int_{t_0}^{t_f} t|e_\lambda|dt+\min_{t,x,e_\lambda}\int_{t_0}^{t_f}\left(q_{13}x^2+q_{14}e_\lambda^{1/5}+q_{15}e_\lambda^2+q_{16}e_\lambda^6\right)dt$$

VLSI efficiency; dynamics (minimum-time); dynamics of the state x and tracking error e_λ transient behavior

$$+\min_V q_{21}\int_{t_0}^{t_f}|V|dt+\min_{t,e_\theta} q_{22}\int_{t_0}^{t_f} t|e_\theta|dt+\min_{t,\theta,e_\theta}\int_{t_0}^{t_f}\left(q_{23}\theta^2+q_{24}e_\theta^{1/5}+q_{25}e_\theta^2+q_{26}e_\theta^6\right)dt, \quad (3)$$

antenna efficiency; dynamics (minimum-time); dynamics of the state θ and tracking error e_θ transient behavior

where t is the time; i is the VCSEL current (we study electrically fed MEMS-based VCSEL); V is the antenna voltage; x is the VCSEL cavity displacement; θ is the beam angular pointing; e_λ and e_θ are the wavelength and tracking errors, $e_\lambda(t)=\lambda_c(t)-\lambda(t)$, $e(t)=\theta_{ref}(t)-\theta(t)$; q_{ij} are the weighting coefficients assigned by the designer.

The nonquadratic objective functional is synthesized using six integrals (terms). In particular, the first and fifth terms maximize the VCSEL and antenna efficiencies penalizing the magnitude of the current and voltage. The second and fifth integrals guarantee the desired transient behavior penalizing the transient time for e_λ and e_θ, e.g., the minimum-time problem. The third and sixth terms ensure the desired dynamics for the linear angular displacement as well as for errors e_λ and e_θ.

It is evident that we design the performance functional using the states, control and outputs variables. The problem is formulated to attain a one-degree-of-freedom beam steering capabilities. However, the Microsystem-on-Chip MOEMS can be synthesized with two-degree-of-freedom nonmechanical beam steering. Using the closed-loop MOEMS response triples (r, y, u), one finds the input-output mapping. This mapping is used in learning, adaptation, reconfiguration, scheduling, and optimization to attain the ultimate goal, e.g., optimize the overall MOEMS performance. The control laws are searched and adapted in the subset of control laws by the *controller optimizer*. Solving the minimization problem, the feedback gains are found within the assigned feedback coefficient intervals by the *feedback gain optimizer*. As the *controller optimizer* defines the control law based upon the best fit and optimal overall performance minimizing the performance functional, the *feedback gain optimizer* searches for the feedback coefficients to be implemented. Thus, we address and study an evolutionary learning-and-controlling concept.

To perform the search, the candidate controller set $\mathbf{K}$ is assigned. In particular, (1) linear and nonlinear proportional-integral-derivative controllers with state feedback, (2) linear quadratic, (3) relay-type control algorithms with *hard-* and *soft-switching*, and (4) sliding mode controllers with *hard-* and *soft-switching* surfaces form the set of controllers.

The weighting coefficients in (3) are assigned to be: $q_{11}=q_{21}=1$, $q_{12}=q_{22}=10$, $q_{13}=q_{23}=1$, $q_{14}=q_{15}=q_{16}=5$ and $q_{24}=q_{25}=q_{26}=10$.

Linear proportional-integral-derivative controllers, linear quadratic, relay-type control algorithms with *hard-switching*, and sliding mode controllers with *hard-switching* do not satisfy the objective functional (3). Thus, these controllers are *improper*, and must be eliminated. The *proper* controllers were obtained as the nonlinear proportional-integral-derivative controller with state feedback, relay-type control with *soft-switching*, and sliding mode controllers with *soft-switching*.

Using the objective functional, the *premium* control algorithm (nonlinear bounded proportional-integral tracking controller) that optimizes the overall MOEMS performance is

$$u_\lambda=\text{sat}\left(-0.87x+14e_\lambda+3.5e_\lambda^{1/5}+6e_\lambda+4.2e_\lambda^5+0.7\int e_\lambda dt\right),$$

$$u_\theta=\text{sat}\left(-0.04\theta+0.9e_\theta^{1/5}+3.5e_\theta+0.84e_\theta^5+8\int e_\theta dt\right).$$

This *premium* controller is bounded and derived from the *proper* controllers. The dynamics of a closed-loop optical MOEMS is shown in Figure 4 for the reference displacements 0.075, 0.0375, 0.11 and 0.075 rad. The analysis of the transient behavior illustrates that the steady-state error is zero, and the settling time is 0.00023 sec.

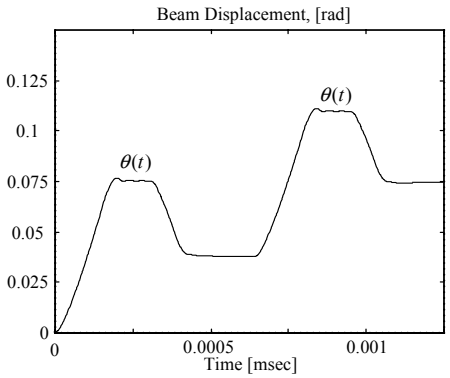

Figure 4. MOEMS dynamics with the *premium* controller

Adaptation and reconfiguration are studied because MOEMS operates in a dynamic environment. It is documented that through learning and adaptation, we maintain the same settling time despite of parameter variations. The results illustrate that while conventional control theory cannot be applied, the documented paradigm allows one to solve a spectrum of very complex problems in control of MOEMS. The synthesized *premium* controller guarantees superior MOEMS performance.

VII. Conclusions

The goal of this paper was to perform fundamental research and developments in devising and designing novel high-performance MOEMS utilizing Microsystem-on-Chip concept. These MOEMS are applicable for high-bandwidth wireless communication, optical interconnect, optical computing, etc. The developed MOEMS that integrate

VCSEL – active optoelectromagnetic microlenses – microdevices – microantennas – ICs can be fabricated using CMOS and surface micromachining technologies. Tunable MEMS-based VCSELs and controlling/processing ICs are directly integrated with the proposed Microsystem-on-Chip solution. In addition to fundamental research (devising MOEMS architectures, synthesis of MOEMS components, high-fidelity modeling, heterogeneous simulations, data-intensive analysis, robust design, and nonlinear optimization), analytic and experimental research was reported. Control of MOEMS is a very difficult problem due to model complexity. We report an intelligent control paradigm for MOEMS. Control laws are designed utilizing evolutionary learning and adaptation with the ultimate objective being to attain the optimal MOEMS performance. The objective functional is evaluated using measured controls, reference (desired beam displacement) and outputs (actual beam displacement and efficiency) as the performance variables.

We designed, tested and characterized the major components (subsystems) of the devised MOEMS. Through these evolutionary and revolutionary developments, the reported results advance core optoelectromagnetics, optoelectromechanics, wireless communication and MOEMS technologies. In particular, the research revolutionizes the state-of-the-art in the integrated optoelectromagnetics and communication with particular applications to military and civilian systems.

The tunable MEMS VCSELs can be used to attain high-bandwidth long-distance wireless optical communication (optical signals can be transmitted through optical fibers or in free-space). The VCSELs are used to attain the lasers-on-chip solution that will have tremendous benefits. The indium gallium arsenide nitride tunable VCSELs with the emission wavelengths from 1.3 to 1.6 μm are applied to attain high-speed data transmission, superior bandwidth, long distance capabilities, and silicon compatibility. The proposed solution leads to hundreds of gigabit per second transmission data rate. These VCSELs are integrated with ICs. The proposed solution guarantees low-power wireless communication at enormous distances due to superior transmitted and radiating power densities. Due to low divergence and high efficiency, VCSELs have the radiating power thousands times higher than any other conventional sources used in wireless communication. Superior pointing accuracy and fast nonmechanical steering are required. Therefore, the proposed MOEMS consists of VCSEL integrated with active optoelectromagnetic microlenses to attain two-degree-of-freedom beam steering capabilities. To model, simulate and analyze integrated complex optoelectromagnetic phenomena and effects, synergetic high-fidelity mathematical models were developed and analyzed. High-fidelity modeling, heterogeneous simulation, and data-intensive analysis lead to design and optimization of high-performance Microsystem-on-Chip MOEMS that guarantee the desired properties and attaining the superior performance (maximal efficiency and robustness, minimal losses and power consumption, long distance, etc.).

REFERENCES

[1] J. M. Kahn, R. H. Katz and K. S. J. Pister, "Emerging challenges: mobile networking for smart dust", *J. Commun. Networks,* vol. 2, no. 3, pp. 188-196, 2000.

[2] J. A. Walker, "MEMS technology in optical layer networks," *Proc. Electronic Components and Technology Conference,* 2001.

[3] R. A. Conant, J. T. Nee, K. Y. Lau and R. S. Muller, "Dynamic deformation of scanning mirrors," *Proc. Optical MEMS Conference*, Kauai, HI, pp. 49-50, 2000.

[4] M.-H. Kiang, O. Solgaard, K.Y. Lau, R.S. Muller, "Electrostatic combdrive-actuated micromirrors for laser-beam scanning and positioning," *Journal of Microelectromechanical Systems*, vol. 7, no. 1., pp. 27-37, 1998.

[5] V. Milanovic, M. Last and K. S. J. Pister, "Laterally actuated torsional micromirrors for large static deflection," *IEEE Photonics Technology Letters*, vol. 15, issue 2, pp. 245-247, 2003.

[6] T. Nee, R. A. Conant, R. S. Muller and K. Y. Lau, "Lightweight, optically flat mirrors for fast beam steering," *Proc. Optical MEMS Conference*, Kauai, HI, 2000.

[7] Z. Lixia, K. S. J. Pister and J. M. Kahn, "Assembled corner-cube retroreflector quadruplet", *Conf. Micro Electro Mechanical Systems*, pp. 556 –559, 2002.

[8] K. T. Gahagan, D. A. Scrymgeour, J. L. Casson, V. Gopalan and J. M. Robinson, "Integrated high-power electro-optic lens and large-angle deflector," *Applied Optics*, vol. 40, no. 31, pp. 5638-5642, 2001.

[9] M. Kulishov, "Tunable electro-optic microlens array. Part I. Planar geometry, Part II. Cylindrical geometry," *Applied Optics*, vol. 39, no. 14, pp. 2332-2339 and vol. 39, no. 20, pp. 3509-3515, 2000.

[10] T. Krupenkin, S. Yang and P. Mach, "Tunable liquid microlens," *Applied Physics Letters*, vol. 82, no. 3, pp. 316-318, 2003.

[11] B. Lofving and S. Hard, "Beam steering with two ferroelectric liquid-crystal spatial light modulators," *Optics Letters*, vol. 23, no. 19, pp. 1541-1543, 1998.

[12] V. Nikulin, V. Skormin and T. Busch "Genetic algorithm optimization for Bragg Cell design," *Optical Engineering Journal*, vol. 41, no. 8, pp. 1767-1773, 2002.

[13] S. E. Lyshevski, *MEMS and MEMS: Systems, Devices, and Structures,* CRC Press, Boca Raton, FL, 2002.

[14] S. E. Lyshevski, "Computational optoelectromechanics and its applications to MEMS VCSELs," *Proc. Conference Material Science and Material Properties for Infrared Optoelectronics*, Kiev, Ukraine, 2002.

[15] C. Z. Ning and P. M. Goorjian, "Microscopic modeling and simulation of transverse-mode dynamics of vertical-cavity surface-emitting lasers," *J. Opt. Soc. America*, vol. 16, no. 11, pp. 2072-2082, 1999.

[16] J. A. Tatum, D Smith, J. K. Guenter and R. H. Johnson "High speed characteristics of VCSELs," *Proc. SPIE,* vol.

3004, 1997.
[17] S. E. Lyshevski and M. Safonov, "Intelligent motion control for electromechanical servos using evolutionary learning and adaptation mechanisms," *Proc. American Control Conf.*, Arlington, VA, pp. 2840-2845, 2001.
[18] M. G. Safonov and T. C. Tsao, "The unfalsified control concept and learning," *IEEE Trans. Automatic Control*, vol. 42, no. 6, pp. 843-847, 1997.